CHEMISTRY
A EUROPEAN JOURNAL

DOI: 10.1002/chem.200501351

Chiral Molecular Magnets: Synthesis, Structure, and Magnetic Behavior of the Series [M(L-tart)] (M = Mn^{II}, Fe^{II}, Co^{II}, Ni^{II}; L-tart = (2*R*,3*R*)-(+)-tartrate)

Eugenio Coronado,* José R. Galán-Mascarós,* Carlos J. Gómez-García, and Ana Murcia-Martínez[a]

Abstract: A new series of layered magnets with the formula [M(L-tartrate)] (M = Mn^{II}, Co^{II}, Fe^{II}, Ni^{II}; L-tartrate = (2*R*,3*R*)-(+)-tartrate) has been prepared. All of these compounds are isostructural and crystallize in the chiral orthorhombic space group *I*222, as found by X-ray structure analysis. Their structure consists of a three-dimensional polymeric network in which each metal shows distorted octahedral coordination bound to four L-tartrate ligands, two of which chelate through an alcohol and a carboxylate group and the other two bind terminally through a monodentate carboxylate group. The chirality of the ligand imposes a Δ conformation on all metal centers. Magnetically, the paramagnetic metal centers form pseudotetragonal layers in which each metal is surrounded by four other metals, with *syn*,*anti* carboxylate bridges. These salts show intralayer antiferromagnetic or ferromagnetic interactions, depending on the electronic configuration of the metal, and weak interlayer antiferromagnetic interaction. In all cases the magnetic properties are strongly affected by the anisotropy of the system, and the presence of magnetic canting has been found. The Mn derivative behaves as a weak ferromagnet with a critical temperature of 3.3 K. The Ni derivative shows very unusual magnetic behavior in that it exhibits antiferromagnetic ordering below 6 K, the onset of spontaneous magnetization arising from spin reorientation into a canted phase below 4.5 K, and a field-induced ferromagnetic state above 0.3 T at 2 K, behavior typical of metamagnets. The Fe and Co derivatives show antiferromagnetic interactions between spin carriers, but do not order above 2 K.

Keywords: chirality · coordination compounds · hydrothermal synthesis · layered compounds · magnetic properties

Introduction

During the last thirty years, coordination chemistry has played a key role in the field of magnetic materials as it has provided many examples of polynuclear metal complexes that serve as models to study exchange interactions, or as materials with useful magnetic properties. In this regard, small ligands that offer a π pathway for the magnetic exchange, like cyanide (CN^-),[1] oxalate ($C_2O_4^{2-}$),[2] dicyanamide ($[N(CN)_2]^-$),[3] or others,[4] are responsible for most of the molecule-based magnets in the literature; the other strategy being the use of spin carriers as ligands for metal centers, such as the organic radicals tetracyanoethylene ($TCNE^-$)[5] and 7,7,8,8-tetracyanoquinodimethane ($TCNQ^-$),[6] or nitronyl nitroxide species.[7] All this background has shown how one can control, at the molecular level, the dimensionality of the magnetic lattice, as well as the sign, strength, and anisotropy of the exchange interactions, providing a useful approach to design novel magnetic molecular materials.

Regarding molecule-based magnetism, two of the most remarkable trends of current interest in the field of materials science are molecular nanomagnets[8,9] and multifunctional magnetic materials.[10–16] The latter are usually constructed from electroactive molecular building blocks that self-assemble into solid architectures, bringing a desired physical prop-

[a] Prof. E. Coronado, Dr. J. R. Galán-Mascarós, Prof. C. J. Gómez-García, A. Murcia-Martínez
Instituto de Ciencia Molecular
Universidad de Valencia
PO Box 22085, 46071 Valencia (Spain)
Fax: (+34) 963-544-859
E-mail: eugenio.coronado@uv.es
jose.r.galan@uv.es

Supporting information for this article is available on the WWW under http://www.chemeurj.org/ or from the author.

erty of interest. Thus, the intermolecular interactions between the molecular fragments will also dictate the existing interactions between both properties. Unusual combinations of properties can be achieved in this way.

One possible combination of properties that has not been thoroughly explored, and where the molecular approach presents many advantages, is that of optical activity and magnetism. Chirality being a property of molecules, it is easy to envision how the use of chiral molecular precursors can lead to the design and preparation of chiral magnetic materials and magnets. The crystal anisotropy caused by the non-centrosymmetric arrangement of the spin carriers may affect the bulk magnetic properties of the material, and even give rise to new phenomena, such as magnetochiral dichroism.[17] Several optically active magnets have been reported over the years. A variety of chiral building blocks have been used to impose chirality into the magnetic networks, including chiral capping ligands,[18] chiral organic radicals,[19] and chiral metal complexes.[20] Some of these have also been obtained from achiral building blocks.[21]

In the search for chiral ligands able to promote magnetic exchange, we focused on the L-tartrate ligand (L-tart). Some tartrate salts have been reported to possess interesting ferroelectric and piezoelectric properties.[22] For a large variety of metals, their tartrate salts are built from a common structural building block, a dimer of general formula $[M_2(L\text{-tart})_2X_n]^{y-}$ (Figure 1), where X can be a solvent molecule or another type of capping ligand.[23] The L-tart ligands chelate the metal centers through the hydroxyl (protonated or deprotonated) and the carboxylate groups, with each metal ion bound to two ligands in *cis* conformation. In the solid state, the divalent metal tartrates afford polymeric structures in which the octahedral coordination geometry of the metal centers is completed by water molecules and by nonchelating carboxylate oxygen atoms from adjacent dimers.[24] When magnetic ions are used, the magnetic intradimer exchange is usually negligible, because the backbone of the L-tart ligand is not very efficient in transmitting the exchange interactions. The interdimer carboxylate bridges, however, can give rise to different magnetic nuclearities depending on the number of solvent molecules substituted by carboxylate O atoms. Among these compounds, only magnetic Cu^{II} dimers[25]and Mn^{II} layers have been characterized.[26] Weak ferromagnetism below the Néel temperature (T_N) = 1.83 K has been reported for the latter.[27]

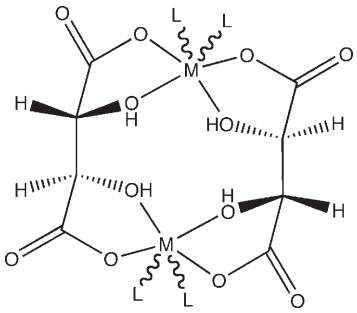

Figure 1. General representation of the molecular structure of the $[M_2L_4(L\text{-tart})_2]$ dimers (L = solvent or other ligands).

Here we report how hydrothermal treatment is a convenient synthetic approach for the preparation of chiral magnetic materials of general formula [M(L-tart)] (M = Mn (**1**), Fe (**2**), Co (**3**), Ni (**4**)) containing two-dimensional magnetic layers. Depending on the nature of the M^{II} metal, this family shows various magnetic behaviors, including unusual magnetic behaviors coming from the chiral character of these compounds.

Abstract in Spanish: *Se ha preparado una nueva serie de imanes isostructurales laminares de fórmula [M(L-tartrato)] (M = Mn^{II}, Co^{II}, Fe^{II}, Ni^{II}; (L-tartrato = (2R,3R)-(+)-tartrato) que cristalizan en el grupo espacial quiral rómbico* I222, *de acuerdo con el anlisis estructural por rayo X. La estructura consiste en una red polimérica 3D donde cada metal posee una coordinacin octaédrica distorsionada unido a cuatro ligandos* L-tartrato, *dos de ellos quelantes a través de un alcohol y de un grupo carboxilato, y dos terminales a través de un grupo carboxilato monodentado. La quiralidad del ligando impone que todos los centros metálicos tenga conformacin Δ. Magnéticamente, los centros metálicos paramagnéticos forman capas pseudo-tetragonales deonde cada metal está rodeado de cuatro metales, con puentes carboxilato* syn anti. *Estas sales muestran interacciones ferromagnéticas o antiferromagnéticas en la capa, dependiendo de la configuración electrónica del metal, e interacciones antiferromagnéticas débiles entre capas. En todos los casos las propiedades magnéticas se ven afectadas por la anisotropía del sistema, encontrándose la presencia de "canting" magnético. El derivado de Mn se comporta como un ferromagneto débil con una temperatura crítica de 3.3 K. El derivado de Ni presenta un comportamiento magnético muy inusual, mostrando ordenamiento antiferromagnético por debajo de 6 K, con la aparición de magnetización espontánea debido a una reorientación de los spines dando lugar a una fase con canting magnético por debajo de 4.5 K, y con un estado ferromagnético inducido por un campo magnético externo por encima de 0.3 T a 2 K, tpico de metamagnetos. Los derivados de Fe y Co muestran interacciones antiferromagnéticas, pero no se ordenan por encima de 2 K.*

Results and Discussion

Synthesis and crystal structure: Compounds [M(L-tart)] (M = Mn (**1**), Fe (**2**), Co (**3**), Ni (**4**)) can be prepared by hydrothermal treatment of solutions containing the metal ions and the ligand. The high temperature and pressure allow for the preparation of these binary compounds, which include no solvent molecules; this favors a higher connectivity between the metal centers and the polydentate ligand. In this

way, instead of chains or planes, a polymeric three-dimensional structure can be formed. The analogous [M(D-tart)] can also be obtained through the same procedure. Circular dichroism measurements confirmed that all products are enantiopure (see Figure S9 in the Supporting Information).

To obtain single crystals of good quality for X-ray diffraction analysis, the oxalate salts of the corresponding metal ions were used. These salts, insoluble at room temperature, are slightly solubilized under hydrothermal conditions and release small quantities of the metals into solution as the reaction takes place. No oxalate is present in the product of the reaction in this case. The best single crystals were obtained with Co^{II}.

The crystal structure of **3** is formed by the $[M_2(L\text{-tart})_2]$ dimer acting as a structural repeating unit. The metal centers are chelated by two tartrate ligands in *cis* orientation, with one O atom from the carboxylate group and another from an adjacent OH group, with each tartrate ligand chelating the two metal centers in the dimer. The structure is then built into a three-dimensional polymer (Figure 2) through the two other coordination positions in the octahedral metal centers that are occupied by oxygen atoms from carboxylate groups from adjacent dimers, thus adopting a *syn*,*anti* bridging mode, far less common than the *syn*,*syn* conformation.[30,31] The octahedra show rhombic distortion, with four M–O short distances (2.046(2) Å) and two longer M–O distances (2.204(2) Å) in *cis* orientation, which correspond to the OH groups (Figure 3). All angles are close to regular octahedra, with the maximum deviation being found for the bite angle of the chelating edge (77.49(8)°). The chirality of the ligands imposes all metal centers to adopt the same Δ conformation. The carboxylate bridges build a pseudotetragonal two-dimensional layer, with each metal center bound to four neighboring metal centers (Figure 4). These layers are held together by the backbone of the tartrate ligands. This well-connected three-dimensional polymer leaves no holes to be occupied by solvent molecules.

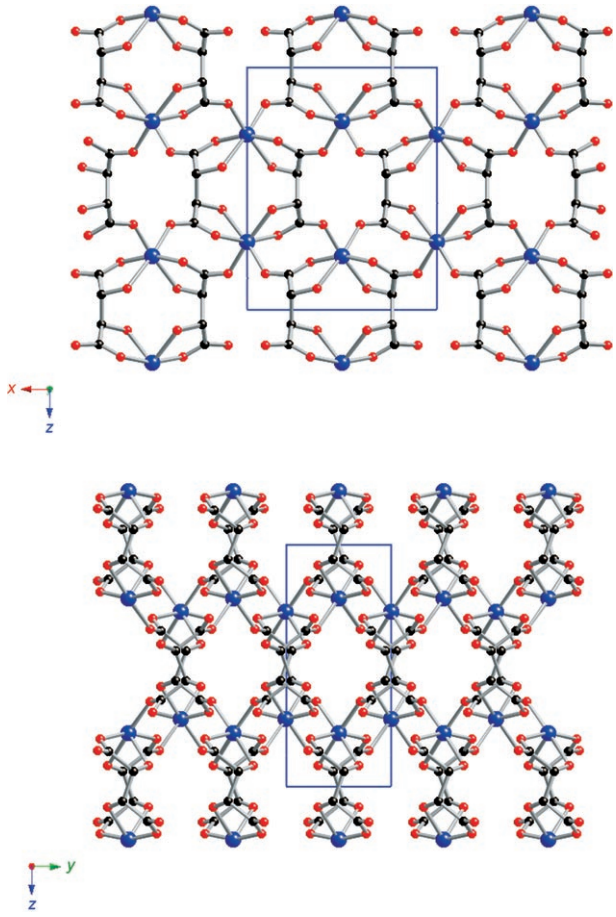

Figure 2. Two different views of the crystal structure of **3**.

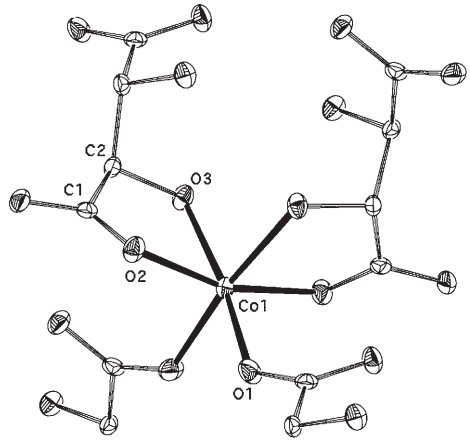

Figure 3. Thermal ellipsoid representation (50% probability) of the crystallographic asymmetric unit in **3**.

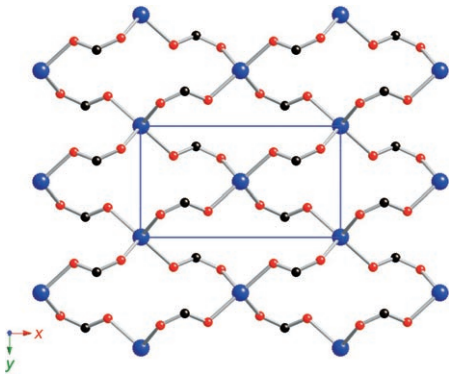

Figure 4. View of the carboxylate-bridged layers, showing the connectivity between metal centers for **3**.

Powder patterns of the rest of the series confirm that all four compounds are isostructural, as concluded from the fact that their powder patterns are in good agreement with the theoretical powder pattern extracted from the single-crystal data obtained for **3**. There are slight differences in the unit-cell parameters (Table 3, see below) among the

series, which follow the trend of metal ion sizes, with Mn^{II} showing the largest unit cell and Ni^{II} the smallest. The corresponding Cu^{II} analogue could not be obtained, because under the same synthetic conditions Cu^{II} is reduced to metallic copper.

Magnetic properties: Magnetically, these salts can be viewed as being formed by two-dimensional magnetic layers, in which all metal centers are connected by *syn,anti* carboxylate bridges. The layers are connected through the backbone of the tartrate ligands, and therefore the superexchange between layers must be negligible.

According to the few examples known, the *syn,anti* carboxylate bridge usually gives rise to weak magnetic exchange, with the magnitude and sign of the exchange depending on the nature of the metal. Ferromagnetic interactions are known to be dominant in Ni^{II}[35–39] and Cu^{II} complexes,[32–34] with very few exceptions for the latter. In turn, antiferromagnetic interactions have been described for Mn^{II} and Co^{II} systems.[40,36,37] Only one example of a Fe^{II} complex with a *syn,anti* bridge has been described, but no magnetic data is available.[41] From these results, it can be deduced that the unpaired spins in e_g orbitals favor ferromagnetic interactions, whereas those in t_{2g} orbitals favor stronger antiferromagnetic interactions, with only one unpaired electron in a t_{2g} orbital being enough to dominate the overall superexchange. Therefore, if Co^{II} is already antiferromagnetic (AF), it is reasonable to expect Fe^{II} to show the same behavior. Our results are in good agreement with these expectations (Table 1).[42]

[Mn(L-tart)] (***1***): Figure 5 shows the magnetic behavior of this salt. In the high-temperature regime (above $T = 50$ K) the $\chi_m T$ product remains almost constant, following the typical paramagnetic Curie–Weiss behavior, for a Curie constant (C) of 4.2 emu K mol^{-1} (C_{SO} = 4.375 emu K mol^{-1}; SO = spin-only) and a Weiss constant (θ) of −6.8 K. The Curie constant has the expected value for an octahedral high-spin Mn^{II} configuration, and the small but negative θ value indicates the presence of AF interactions between the Mn^{II} centers. The negative Weiss parameter can be used to estimate the value of the interaction by using the mean-field expression $\theta = zJS(S+1)/3k_B$, where z is the number of nearest neighbors, J is the angular momentum, S is the spin angular momentum, and k_B is the Boltzmann constant. This yields $J/k_B = -0.41$ cm^{-1} (−0.58 K), for $z = 4$.

Due to this interaction, the $\chi_m T$ product shows a rapid decrease below $T = 50$ K, while χ_m tends to a maximum at

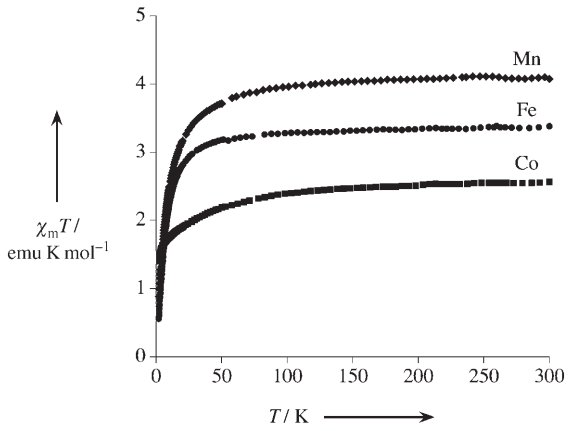

Figure 5. Temperature dependence of the $\chi_m T$ product for **1**, **2**, and **3** at 0.1 T.

$T = 4$ K (see Figure S2 in the Supporting Information). Directly below this temperature, χ_m shows a jump and reaches saturation below $T = 3$ K, suggesting the presence of a magnetically ordered state with a net magnetization arising from uncompensated spins. Because the near-neighbor interactions are antiferromagnetic, the spontaneous magnetization must arise from the presence of canting between the antiparallel alignment of the spins, as typically observed for a weak ferromagnet. This is confirmed by the dynamic (ac) magnetic susceptibility measurements (Figure 6) that show a maximum in the in-phase (χ'_m), and a peak in the out-of-phase signal (χ''_m) that becomes nonzero at 3.3 K, defining the temperature of magnetic ordering and confirming the presence of net magnetization in the ordered state. This peak shows a very broad shoulder with its maximum around $T = 3$ K, which also appears in the plot of χ'_m. The shoulder is frequency dependent (Figure 6), and disappears for frequencies above 100 Hz, whereas the position of the main peak remains unchanged. This suggests that the shoulder is related to dynamic effects, such as domain wall movement, while the peak corresponds to the magnetic ordering. Similar features have already been observed in the ac susceptibility behavior of other low-dimensional molecular magnets (most of them two dimensional).[28] At 2 K, the field dependence of the magnetization increases monotonically, reaching values far from saturation even at $H = 5$ T (see Figure S3 in the Supporting Information), and shows a hysteresis loop with a coercive field (H_{coer}) of 45 mT (see Figure S4 in the Supporting Information).

[Fe(L-tart)] (***2***): In the high-temperature regime, salt **2** shows magnetic behavior analogous to **1** (Figure 5). It follows a Curie–Weiss law with C = 3.20 emu K mol^{-1} (C_{SO} = 3.0 emu K mol^{-1}) and θ = −5.8 K (J = −0.50 cm^{-1}), which suggest the presence of

Table 1. Main magnetic parameters for the salts [M(L-tart)].

M	S	C [emu K mol^{-1}]	g	θ [K]	J [cm^{-1}]	Ordering	T_c[a] [K]	H_{coer}[b] [mT]	M_R[c] [μ_B]
Mn	5/2	4.2	1.96	−6.8	−0.40	WF	3.3	45	0.03
Fe	2	3.2	2.07	−5.8	−0.50	–	–	–	–
Co	"3/2"	2.7	2.38	−11.03	−2.21	–	–	–	–
Ni	1	1.0	2.00	+4.2	+1.58	AF/WF	6/4.5	60	0.07

[a] Critical temperature. [b] At $T = 2$ K. [c] M_R = remnant magnetization.

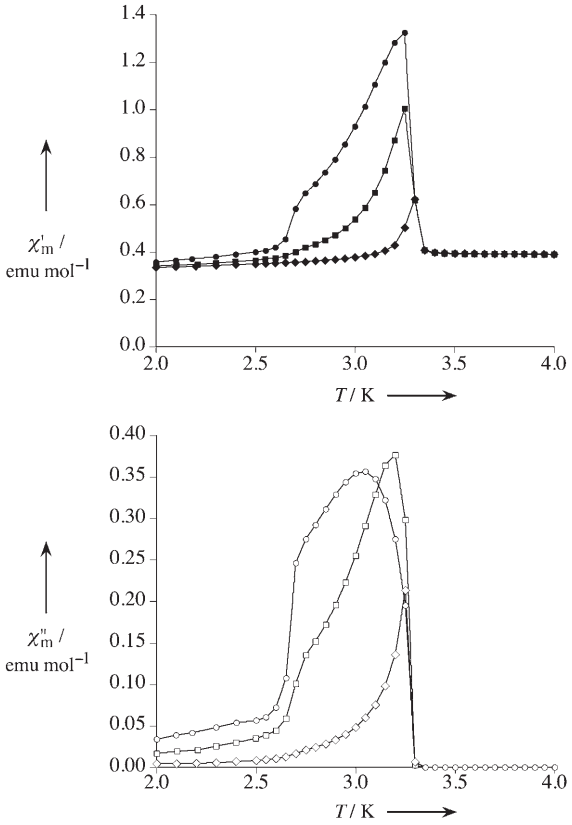

Figure 6. Temperature dependence of the ac magnetic susceptibilities (χ'_m = in phase, χ''_m = out of phase) for **1** at 10 (●/○), 100 (■/□), and 1000 Hz (◆/◇).

AF interactions. The decrease in $\chi_m T$ is also very rapid below $T = 50$ K, but no sign of magnetic ordering appeared above $T = 2$ K, the limit for our measurements. The field dependence of the magnetization (see Figure S3 in the Supporting Information) is similar to that of **1** with a slight curvature, but also remaining far from saturation at high fields.

*[Co(L-tart)] (**3**)*: In this case, the $\chi_m T$ product exhibits a continuous decrease from room temperature. The magnetic moment at room temperature is very high ($\chi_m T$ = 2.52 emu K mol^{-1}) when compared with the expected spin-only value (C_{SO} = 1.875 emu K mol^{-1}). Above $T = 50$ K the magnetic data can be fitted to a Curie–Weiss law with C = 2.7 emu K mol^{-1} and $\theta = -11.03$ K ($J = -2.21$ cm^{-1}). These parameters are obviously too high as they account for the dominant anisotropy of the octahedral Co^{II} centers and also for the magnetic exchange. Thus, we can only conclude that the magnetic exchange must be very weak, and probably also antiferromagnetic, because the $\chi_m T$ product keeps decreasing down to very low temperatures. The field dependence of the magnetization supports this conclusion, with a slow increase of the magnetization, although in this case the compound tends to saturation above $H = 3$ T, to a value lower than expected (2.5 μ_B). This suggests, as already discussed, that the antiferromagnetic interactions are weaker in this case, relative to the other derivatives, and also confirms the presence of canting between local spins, even when the field tends to force their parallel alignment.

*[Ni(L-tart)] (**4**)*: The magnetic behavior of salt **4** is different from the other members of the series, as expected. The thermal variation of the $\chi_m T$ product at $H = 0.1$ T shows a small but continuous increase when decreasing the temperature (Figure 7) that fits a Curie–Weiss law above 50 K with

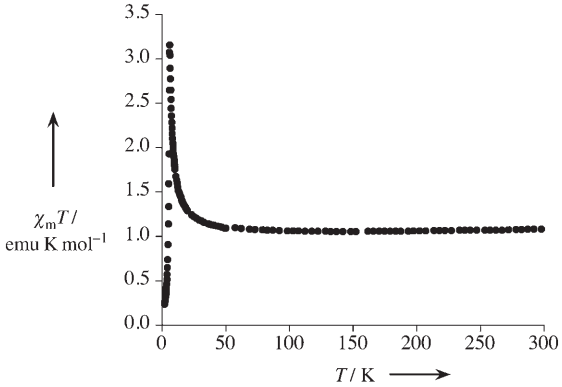

Figure 7. Temperature dependence of the $\chi_m T$ product for **4**.

$C = 1.01$ emu K mol^{-1} and $\theta = +4.2$ K ($J = +1.58$ cm^{-1}); this indicates the presence of ferromagnetic interactions between the near-neighbor paramagnetic metal centers through the *syn*,*anti* carboxylate bridge. Below 50 K, $\chi_m T$ increases sharply and reaches a maximum value around T = 6 K ($\chi_m T$ = 3.2 emu K mol^{-1}) and then decreases also very rapidly. The abrupt increase below 50 K arises from the large correlation between the magnetic moments in the layer.

In the low temperature range χ_m also shows a sharp maximum at $T = 6$ K with an applied field of 0.1 T, which is the signature of antiferromagnetic ordering. Heat-capacity measurements have also been performed (see Figure S5 in the Supporting Information) that show a sharp lambda peak that confirms the presence of magnetic ordering, with its maximum at 6 K defining T_N. This ordering must be triggered by weak antiferromagnetic interactions between the largely correlated ferromagnetic layers in the solid, which are only 5.15 Å apart. At higher fields the χ_m maximum shifts towards lower temperatures and completely disappears for fields over $H = 0.6$ T, where χ_m increases continuously reaching saturation of the magnetization below T = 4 K (see Figure S6 in the Supporting Information). This behavior is typical of metamagnets, for which a critical external magnetic field breaks the antiferromagnetic ordering and induces the appearance of a ferromagnetic phase. The field dependence of the magnetization at $T = 2$ K confirms this point. Thus, the magnetization (M) has a sigmoidal shape, with a linear, slow increase for small fields, as expected for a sample with dominant AF interactions, and with a sudden change in slope above $H = 0.3$ T, which defines the

critical field needed to overcome the antiparallel alignment of the spins at $T = 2$ K (Figure 8). From magnetization measurements at different temperatures (see Figure S7 in the Supporting Information) it was found that this critical field decreases for higher temperatures reaching the value of zero for T_N.

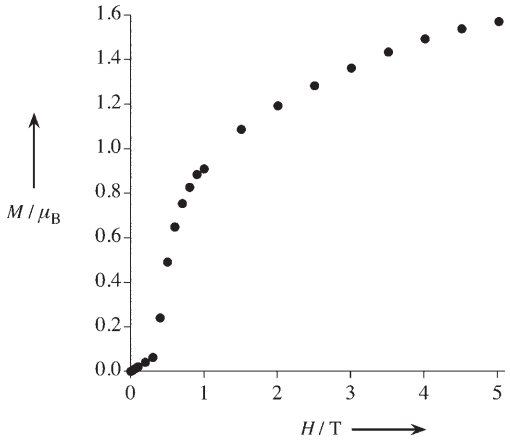

Figure 8. Field dependence of the magnetization for **4** at $T = 2$ K.

The presence of a field-induced ferromagnetic phase[43] is also confirmed by the hysteretic behavior of the field dependence of the magnetization (Figure 9), which shows a hysteresis loop of 0.1 T above $H = 0.3$ T at 2 K. The width of this hysteresis loop decreases when the temperature is increased, and vanishes at 4.5 K, indicating that above this temperature and below T_N there is a field-induced paramagnetic phase. Surprisingly, there is a second hysteresis loop in the $T = 2$–4.5 K range that appears in the "antiferromagnetic" phase, with a maximum width of 60 mT at 2 K. Such behavior is unusual of metamagnets, although it has already been observed in molecule-based materials.[44]

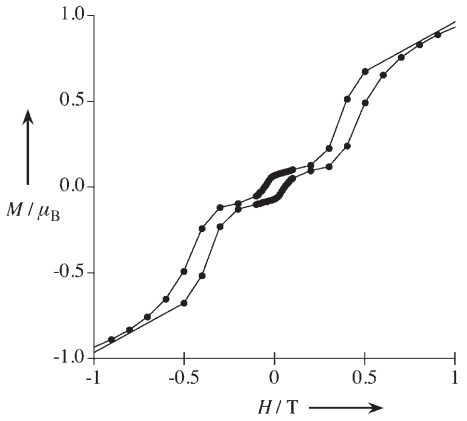

Figure 9. Hysteresis loop of the magnetization at $T = 2$ K for **4**.

Dynamic (ac) magnetic susceptibility measurements were also performed (Figure 10). χ'_m has a maximum at $T = 6$ K, equivalent to that observed in the static (dc) data, with a small shoulder around $T = 4.5$ K. χ''_m remains essentially null[45] but it becomes nonzero at $T = 4.5$ K with the appearance of a weak and slightly frequency dependent peak with its maximum around $T = 4$ K that corresponds to the small shoulder observed in χ'_m. This indicates the onset of spontaneous magnetization in the system below $T = 4.5$ K that must arise from a spin reorientation from a pure antiferromagnetic phase to a spin-canted phase. This second magnetic transition is not related to any feature in the specific heat data, thus indicating that the entropy associated with this process is very weak. Such a case has already been reported for other molecule-based materials that present two different magnetic transitions, where the one that occurs at higher temperature always dominates the specific heat capacity and the second one has almost no effect.[46] In our case, this second transition affords a very small increase in χ'_m, and also a very small, almost negligible, increase in the field dependence of the magnetization for small fields, which depends on the effective canting angle between antiparallel spins in a weak ferromagnet. This suggests that the canting angle must be very small too. The zero-field-cooled

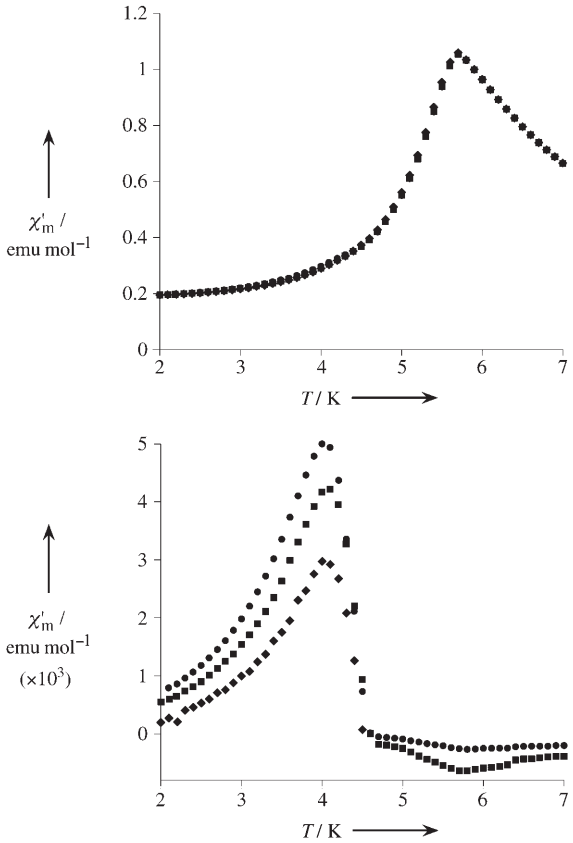

Figure 10. Temperature dependence of the ac magnetic susceptibilities (χ'_m = in phase, χ''_m = out of phase) for **4** at 10 (●), 100 (■), and 1000 Hz (◆).

(ZFC), field-cooled (FC), and remnant magnetization measurements with an applied field of 25 G (see Figure S8 in the Supporting Information) are in good agreement with this hypothesis. ZFC and FC measurements are completely identical above $T = 4$ K, both of them showing the same maximum in χ_m. Below 4 K the ZFC behavior clearly deviates from that of FC, confirming the appearance of spontaneous magnetization. The remnant magnetization becomes zero at this same critical temperature.

With all this data we have been able to determine the phase diagram for this material (Figure 11). It reaches AF ordering with a T_N of 6 K owing to weak antiferromagnetic

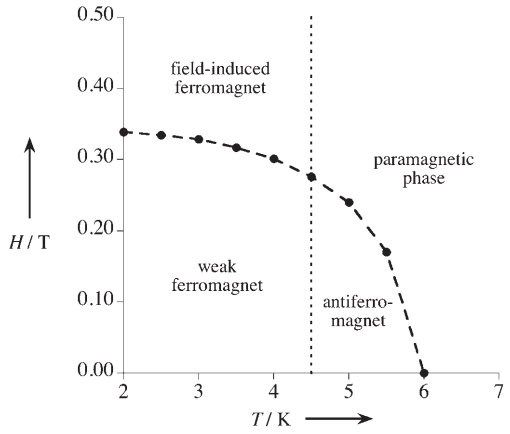

Figure 11. Phase diagram for **4**.

interactions between the ferromagnetically correlated layers. A second magnetic transition to weak ferromagnet occurs at $T = 4.5$ K, arising from the onset of spin canting. The magnetic ordering can be overcome by an external magnetic field that induces a ferromagnetically ordered phase or a paramagnetic phase, below or above 4.5 K, respectively.

Conclusion

We have shown how the molecular approach can be used to obtain optically active magnetic materials, from the use of chiral polydentate ligands that act as mediators for the magnetic exchange while imposing chirality on the metal centers. In particular, the hydrothermal synthesis is a useful procedure to obtain solvent-free coordination compounds, as the connectivity of the system increases. A series of isostructural binary compounds from first-row metal ions and the L-tartrate ligand have been prepared and characterized. With the same structural features in this homometallic series, the paramagnetic metal ions are connected to each other through *syn*,*anti* carboxylate bridges to form magnetic layers. Antiferromagnetic interactions are favored in the Mn, Fe, and Co analogues, while Ni favors ferromagnetic interactions. Among the antiferromagnetic examples, only the Mn derivative presents strong enough magnetic exchange to show magnetic ordering above $T = 2$ K. The presence of canting between the spin carriers prevents the appearance of pure AF three-dimensional ordering, and this material behaves as a weak ferromagnet with spontaneous magnetization observed below $T = 3.3$ K. The Ni derivative shows quite unusual and complex magnetic behavior. The ferromagnetic layers are antiferromagnetically coupled in the solid state thus promoting antiferromagnetic ordering at $T = 6$ K and overall metamagnetic behavior. In addition, the anisotropy of the material induces the appearance of net magnetization below $T = 4.5$ K due to the occurrence of a second transition into a spin-canted antiferromagnetic phase. This complex behavior is unprecedented in molecule-based systems.

Although several magnets with chiral crystal structures are known, as discussed in the introduction, the magnetic structure is rarely chiral,[47] and little effect, if any, is observed on the magnetic properties. In this case, we have found rather peculiar magnetic phenomena in this series, but still it is an open question as to whether the magnetic structure of these materials is chiral, as their behavior suggests. To confirm this point, neutron diffraction experiments are underway.

Another interesting investigation will focus on the possible relation between optical and magnetic properties. These materials appear as good candidates to study the so-called optical magnetochiral anisotropy,[17] never observed for a magnet. The lack of large enough single crystals and the low temperatures at which spontaneous magnetization arises put a limit on the optical studies that can be performed at the moment.

This strategy can also be extended to other chiral polydentate ligands, with particular interest on the introduction of functional groups able to promote stronger magnetic exchange, such as oxo or hydroxo groups. The aim would be to reach higher critical temperatures for the observation of these unusual magnetic features.

Experimental Section

Materials: All reagents and solvents were used as purchased.

Syntheses

*[Mn(L-tart)$_3$] (**1**)*: $Mn(CH_3COO)_2{\cdot}4H_2O$ (0.49 g, 2 mmol) and L-KH(tart) (1.5 g, 8 mmol) were suspended in water (30 mL) and heated in a Teflon autoclave at 180 °C for 10 days. Compound **1** was filtered off, dried in air at room temperature, and obtained as a polycrystalline white powder (215 mg, 53 %). Elemental analysis calcd (%) for $C_4H_4MnO_6$ (M_r = 203.01): C 23.67, H 1.99; found: C 23.81, H 1.95.

*[Fe(L-tart)$_3$] (**2**)*: This was prepared by using the same procedure as that for **1** but with $Fe(SO_4){\cdot}7H_2O$ (0.56 g, 2 mmol) as the starting material instead. Compound **2** was obtained as a polycrystalline light yellow powder (169 mg, 40 %). Elemental analysis calcd (%) for $C_4H_4FeO_6$ (M_r = 203.92): C 23.56, H 1.98; found: C 23.86, H 2.02.

*[Co(L-tart)$_3$] (**3**)*: This was prepared by following the same procedure mentioned above but using $Co(CH_3COO)_2{\cdot}4H_2O$ (0.50 g, 2 mmol) as the starting material instead, to give **3** as a polycrystalline purple powder (200 mg, 50 %). Elemental analysis calcd (%) for $C_4H_4CoO_6$ (M_r = 206.93): C 23.21, H 1.95; found: C 23.33, H 1.99. Purple prismatic single

crystals of this compound were obtained by following the same procedure but using Co(ox)·2 H_2O (0.36 g, 2 mmol) as the starting reagent instead.

*[Ni(L-tart)$_3$] (**4**)*: This was prepared by following the above-mentioned procedure using $Ni(CH_3COO)_2$·4 H_2O (0.50 g, 2 mmol) as the starting material to give **4** as a polycrystalline light green powder (280 mg, 67 %). Elemental analysis calcd (%) for $C_4H_4NiO_6$ (M_r = 206.77): C 23.24, H 1.95; found: C 22.99, H 2.06.

X-ray crystallography: A purple prismatic single crystal of **3** (0.3 × 0.3 × 0.2 mm) was fixed onto a glass fiber with epoxy glue and mounted on a KappaCCD diffractometer that uses graphite-monochromated $Mo_{K\alpha}$ radiation (λ = 0.71073). Cell refinements and data reduction were performed at T = 120 K using the Denzo and Scalepack programs.[48] The structure was solved by direct methods using the SIR97 program,[49] and refined on F^2 with the SHELXL-97 program.[50] All non-hydrogen atoms were found after successive Fourier difference analysis and refined anisotropically. H atoms were located in their calculated positions. Crystallographic data and the main refinement parameters are presented in Table 2. CCDC-230223 contains the supplementary crystallographic data for this paper. These data can be obtained free of charge from the Cambridge Crystallographic Data Center via www.ccdc.cam.ac.uk/data_request/cif.

Table 2. Main structural parameters and crystallographic data for the salt [Co(L-tart)] (**3**).

formula	$C_4H_4CoO_6$
M_r	207.00
space group	*I*222
a [Å]	9.117(3)
b [Å]	5.057(2)
c [Å]	11.631(3)
V [Å^3]	536.2(3)
Z	4
T [K]	120(2)
λ [Å]	0.71073
ρ_{calcd} [g cm^{-3}]	2.564
μ [mm^{-1}]	3.173
θ range	2.84–27.47
reflections total	608
reflections [$I > 2\sigma(I)$]	563
parameters	51
$R1$[a]	0.0321
$wR2$[a]	0.0475

[a] $R1 = \Sigma(F_o - F_c)/\Sigma(F_o)$, $wR2 = [\Sigma[w(F_o^2 - F_c^2)^2]/\Sigma[w(F_o^2)^2]]^{1/2}$; $w = 1/[\sigma^2(F\sigma^2) + (0.009P)^2 + 0.1799P]$ in which $P = (F_o^2 + 2F_c^2)/3$.

The X-ray powder diffraction patterns for **1**, **2**, and **4** were recorded at room temperature with a Siemens D-500 powder diffractometer ($Cu_{K\alpha}$) in the 2θ range of 2–60° (with steps of 0.02° and a measuring time of 15 s). These patterns are consistent with the theoretical powder pattern calculated from the single-crystal solution found for **3**,[52] which confirms that all four compounds are isostructural (see Figure S1 in the Supporting Information). Experimental unit cells were obtained by indexation of the reflections in a orthorhombic space group with the UnitCell program.[51] Unit-cell parameters are summarized in Table 3.

Physical measurements: Magnetic measurements were carried out with a Quantum Design (SQUID) Magnetometer MPMS-XL-5. The dc measurements were performed with applied fields of up to 5000 G (0.5 T) in the 2–300 K temperature range. The ac measurements were performed with an alternating field of 3.95 G (3.95×10^{-4} T) at different frequencies between 1 and 1000 Hz. Data were corrected for the diamagnetic contributions by using Pascal constants. Calorimetric measurements were carried out on pressed pellets with a Quantum Design PPMS in the range T = 2–15 K. Circular dichroism absorption spectra were measured on KBr pressed pellets and recorded with a Jasco J810 spectropolarimeter.

Table 3. Experimental unit-cell parameters for the salts [M(L-tart)].

M	a [Å]	b [Å]	c [Å]	V [Å^3]
Mn	9.40(2)	5.054(6)	11.665(9)	554.4(8)
Fe	9.241(11)	5.016(5)	11.617(13)	538.4(6)
Co[a]	9.093(5)	5.046(3)	11.608(5)	532.6(3)
Ni	8.989(8)	4.988(4)	11.460(9)	513.9(4)

[a] From powder diffraction data.

Acknowledgements

This work was supported by the Ministerio de Educación y Ciencia (projects MAT2004-3849 and BQU2002-01091), and the Generalitat Valenciana (GV04A/77). A.M.M. thanks the Ministerio de Educación y Ciencia for a predoctoral fellowship.

[1] K. R. Dunbar, R. A. Heintz, *Prog. Inorg. Chem.* **1997**, *45*, 283–391.
[2] a) H. Tamaki, Z. J. Zhong, N. Matsumoto, S. Kida, M. Koikawa, N. Achiwan, Y. Hashimoto, H. Okawa, *J. Am. Chem. Soc.* **1992**, *114*, 6974–6979; b) C. Mathonière, C. J. Nuttall, S. G. Carling, P. Day, *Inorg. Chem.* **1996**, *35*, 1201–1206; c) E. Coronado, J. R. Galán-Mascarós, C. J. Gómez-García, J. Ensling, P. Gütlich, *Chem. Eur. J.* **2000**, *6*, 552–563.
[3] a) M. Kurmoo, C. J. Kepert, *New J. Chem.* **1998**, *22*, 1515–1524; b) J. L. Manson, C. R. Kmety, Q. Z. Huang, J. W. Lynn, G. M. Bendele, S. Pagola, P. W. Stephens, L. M. Liable-Sands, A. L. Rheingold, A. J. Epstein, J. S. Miller, *Chem. Mater.* **1998**, *10*, 2552–2560; c) S. R. Batten, K. S. Murray, *Coord. Chem. Rev.* **2003**, *246*, 103–130; d) S. R. Batten, P. Jensen, B. Moubaraki, K. S. Murray, R. Robson, *Chem. Commun.* **1998**, 430–440.
[4] J. R. Galán-Mascarós, K. R. Dunbar, *Angew. Chem.* **2003**, *115*, 2391–2395; *Angew. Chem. Int. Ed.* **2003**, *42*, 2289–2293.
[5] J. M. Manriquez, G. T. Yee, R. S. McLean, A. J. Epstein, J. S. Miller, *Science* **1991**, *252*, 1415–1417.
[6] a) H. Zhao, M. J. Bazile, J. R. Galán-Mascaróa, K. R. Dunbar, *Angew. Chem.* **2003**, *115*, 1045–1048; *Angew. Chem. Int. Ed.* **2003**, *42*, 1015–1018; b) R. Clérac, S. O'Kane, J. Cowen, X. Ouyang, R. Heintz, H. Zhao, M. J. Bazile, Jr., K. R. Dunbar, *Chem. Mater.* **2003**, *15*, 1840–1850.
[7] H. O. Stumpf, L. Ouahab, Y. Pei, P. Bergerat, O. Kahn, *J. Am. Chem. Soc.* **1994**, *116*, 3866–3874.
[8] a) R. Sessoli, H.-T. Tsai, A. R. Schake, S. Wang, J. B. Vincent, K. Folting, D. Gatteschi, G. Christou, D. N. Hendrickson, *J. Am. Chem. Soc.* **1993**, *115*, 1804–1816; b) R. Sessoli, D. Gatteschi, A. Caneschi, M. A. Novak, *Nature* **1993**, *365*, 141–143.
[9] A. Caneschi, D. Gatteschi, N. Latioti, C. Sangregorio, R. Sessoli, G. Venturi, A. Vindigni, A. Rettori, M. G. Pini, M. Novak, *Angew. Chem.* **2001**, *113*, 1810–1813; *Angew. Chem. Int. Ed.* **2001**, *40*, 1760–1763.
[10] E. Coronado, J. R. Galán-Mascarós, C. J. Gómez-García, V. Laukhin, *Nature* **2000**, *408*, 447–449.
[11] A. Alberola, E. Coronado, J. R. Galán-Mascarós, C. Giménez-Saiz, C. J. Gómez-García, *J. Am. Chem. Soc.* **2003**, *125*, 10774–10775.
[12] E. Coronado, J. R. Galán-Mascarós, C. J. Gómez-García, E. Martínez-Ferrero, S. van Smaalen, *Inorg. Chem.* **2004**, *43*, 4808–4810.
[13] M. Kurmoo, A. W. Graham, P. Day, S. J. Coles, M. B. Hursthouse, J. M. Caulfield, J. Singleton, L. Ducasse, P. Guionneau, *J. Am. Chem. Soc.* **1995**, *117*, 12209–12217.
[14] H. Kobayashi, A. Sato, E. Arai, H. Akutsu, A. Kobayashi, P. Cassoux, *J. Am. Chem. Soc.* **1997**, *119*, 12392–12393.
[15] a) O. Sato, T. Iyoda, A. Fujishima, K. Hashimoto, *Science* **1996**, *272*, 704–705; b) O. Sato, Y. Einaga, A. Fujishima, K. Hashimoto, *Inorg. Chem.* **1999**, *38*, 4405–4412.
[16] a) S. Bénard, P. Yu, J. P. Audiére, E. Riviére, R. Clèment, J. Ghilhem, L. Tchertanov, K. Nakatani, *J. Am. Chem. Soc.* **2000**, *122*,

9444–9454; b) S. Bénard, E. Riviére, P. Yu, K. Nakatani, J. F. Delouis, *Chem. Mater.* **2001**, *13*, 159–162.
[17] G. L. J. A. Rikken, E. Raupach, *Nature* **1997**, *390*, 493–494.
[18] a) H. Imai, K. Inoue, K. Kikuchi, Y. Yoshida, M. Ito, T. Sunahara, S. Onaka, *Angew. Chem.* **2004**, *116*, 5736–5739; *Angew. Chem. Int. Ed.* **2004**, *43*, 5618–5621; b) K. Inoue, H. Imai, P. S. Ghalsasi, K. Kikuchi, M. Ohba, H. Okawa, J. V. Yakhmi, *Angew. Chem.* **2001**, *113*, 4372–4375; *Angew. Chem. Int. Ed.* **2001**, *40*, 4242–4245; c) E. Coronado, C. J. Gómez-García, A. Nuez, F. M. Romero, E. Rusanov, H. Stoeckli-Evans, *Inorg. Chem.* **2002**, *41*, 4615–4617.
[19] M. Minguet, D. Luneau, E. Lhotel, V. Villar, C. Paulsen, D. B. Amabilino, J. Veciana, *Angew. Chem.* **2002**, *114*, 606–609; *Angew. Chem. Int. Ed.* **2002**, *41*, 586–588.
[20] a) E. Coronado, J. R. Galán-Mascarós, C. J. Gómez-García, E. Martínez-Ferrero, M. Almeida, J. C. Waerenborgh, *Eur. J. Inorg. Chem.* **2005**, 2064–2070; b) E. Coronado, J. R. Galán-Mascarós, C. J. Gómez-García, J. M. Martínez-Agudo, *Inorg. Chem.* **2001**, *40*, 113–120; c) R. Andres, M. Brissard, M. Gruselle, C. Train, J. Vaissermann, B. Malezzieux, J. P. Jamet, M. Verdaguer, *Inorg. Chem.* **2001**, *40*, 4633–4640.
[21] a) E. Q. Gao, Y. F. Yue, S. Q. Bai, Z. He, C. H. Yan, *J. Am. Chem. Soc.* **2004**, *126*, 1419–1429; b) D. Armentano, G. DeMunno, F. Lloret, A. V. Palli, M. Julve, *Inorg. Chem.* **2002**, *41*, 2007–2013.
[22] M. E. Torres, T. López, J. Peraza, J. Stockel, A. C. Yanes, C. Gonález-Silgo, C. Ruiz-Pérez, P. A. Lorenzo-Luis, *J. Appl. Phys.* **1998**, *84*, 5729–5732.
[23] a) M. Nakahanada, T. Fujihara, N. Koine, S. Kaizaki, *J. Chem. Soc. Dalton Trans.* **1992**, 3423–3426; b) D. Bayot, B. Tinant, M. Devillers, *Inorg. Chem.* **2005**, *44*, 1554–1562.
[24] a) L. J. Bostelaar, R. A. G. de Graaff, F. B. Hulsbergen, J. Reedijk, W. M. H. Sachtler, *Inorg. Chem.* **1984**, *23*, 2294–2297; b) C. González-Silgo, J. González-Platas, C. Ruiz-Pérez, T. López, M. E. Torres, *Acta Crystallogr. Sect. C* **1999**, *55*, 710–712.
[25] a) V. H. Crawford, W. E. Hatfield, *J. Mol. Struct.* **1977**, *37*, 157–159;
[26] C. Ruiz-Pérez, M. Hernández-Molina, C. González-Silgo, T. López, C. Yanes, X. Solans, *Acta Crystallogr. Sect. C* **1996**, *52*, 2473–2475.
[27] A. Paduan-Filho, C. C. Becerra, *J. Phys. Condens. Matter* **2000**, *12*, 2071–2078.
[28] a) F. Bellouard, M. Clemente-León, E. Coronado, J. R. Galán-Mascarós, C. J. Gómez-García, F. M. Romero, K. R. Dunbar, *Eur. J. Inorg. Chem.* **2002**, 1603–1606; b) F. Thétiot, S. Triki, J. Sala-Pala, C. J. Gómez-García, S. Golhen, *Chem. Commun.* **2002**, 1078–1079.
[29] R. Pellaux, H. W. Schmalle, R. Huber, P. Fisher, T. Hauss, B. Ouladdiaf, S. Decurtins, *Inorg. Chem.* **1997**, *36*, 2301–2308.
[30] G. B. Deadon, R. J. Phillips, *Coord. Chem. Rev.* **1980**, 227–250.
[31] R. L. Rardin, W. B. Tolman, S. J. Lippart, *New J. Chem.* **1991**, *15*, 417–430.
[32] E. Colacio, M. Ghazi, R. Kivekäs, J. M. Moreno, *Inorg. Chem.* **2000**, *39*, 2882–2890.
[33] K. K. Nanda, A. W. Addison, E. Sinn, L. K. Thompson, *Inorg. Chem.* **1996**, *35*, 5966–5967.
[34] D. Schultz, T. Weyhermüller, K. Wieghartdt, C. Butzlaff, A. X. Trautwein, *Inorg. Chim. Acta* **1996**, *247*, 387–394.
[35] F.-T. Xie, L.-M. Duan, J.-Q. Xu, L. Ye, Y.-B. Liu, X.-X. Hu, J.-F. Song, *Eur. J. Inorg. Chem.* **2004**, 4375–4379.
[36] T. Whitfield, L.-M. Zheng, X. Wang, A. J. Jacobson, *Solid State Sci.* **2001**, *3*, 829–835.
[37] F. S. Delgado, M. Hernández-Molina, J. Sanchiz, C. Ruiz-Pérez, Y. Rodríguez-Martín, T. López, F. Lloret, M. Julve, *CrystEngComm* **2004**, *6*, 106–111.
[38] P. S. Mukherjee, S. Konar, E. Zangrando, T. Mallah, J. Ribas, N. R. Chaudhuri, *Inorg. Chem.* **2003**, *42*, 2695–2703.
[39] M. Du, X. H. Bu, Y. M. Guo, L. Zhang, D. Z. Liao, J. Ribas, *Chem. Commun.* **2002**, 1478–1479.
[40] K. O. Kongshaug, H. Fjellvåg, *Solid State Sci.* **2002**, *4*, 443–447.
[41] J. Kozelka, B. Spingler, S. J. Lippard, *Inorg. Chim. Acta* **2002**, *337*, 212–222.
[42] The magnetic properties discussed here for the [M(L-tartrate)] derivatives are completely identical to those of their [M(D-tartrate)] counterparts.
[43] A. Marvilliers, S. Parsons, E. Rivire, J.-P. Audire, M. Kurmoo, T. Mallah, *Eur. J. Inorg. Chem.* **2001**, 1287–1293.
[44] G. T. Yee, M. J. Whitton, R. D. Sommer, C. M. Frommen, W. M. Reiff, *Inorg. Chem.* **2000**, *39*, 1874–1877.
[45] At high frequencies a very weak negative peak was observed at $T = 5.9$ K in the out-of-phase signal, which shows a strong frequency dependence of its intensity, but not of its position. Such a result is surprising, because a negative χ''_m signal does not have a clear physical meaning. This, along with the fact that the intensity of the in-phase signal is several orders of magnitude larger, leads us to assign this negative peak to an artifact of the measurement, probably due to a nonperfect alignment of the experimental setup for the magnetic ac measurements, although this result has been reproducibly observed in measurements performed with two different Quantum Design SQUID Susceptometers and also with a Quantum Design PPMS. We want to note, however, that negative features in χ''_m have already been reported for some magnets, and assigned in those cases to anomalous relaxation processes in the following, for example: E. M. Levin, V. K. Pecharsky, K. A. Gschneidner, Jr., *J. Appl. Phys.* **2001**, *90*, 6255–6262.
[46] a) J. Larionova, O. Kahn, S. Gohlen, L. Ouahab, R. Clérac, *J. Am. Chem. Soc.* **1999**, *121*, 3349–3356; b) J. Larionova, R. Clérac, J. Sanchiz, O. Kahn, S. Golehn, L. Ouahab, *J. Am. Chem. Soc.* **1998**, *120*, 13088–13095.
[47] R. Feyerherm, A. Loose, T. Ishida, T. Nogami, J. Kreitlow, D. Baabe, F. J. Litterst, S. Süllow, H.-H. Klauss, K. Doll, *Phys. Rev. B* **2004**, *69*, 134427.
[48] Z. Otwinowski, W. Minor, in *Methods in Enzymology, Vol. 276* (Eds.: C. W. Carter, Jr., E. M. Sweet), Academic Press, **1997**, pp. 307–326.
[49] SIR97: A. Altomare, M. C. Burla, M. Camali, G. L. Cascarano, C. Giacovazzo, A. Guagliardi, A. G. G. Moliterni, G. Polidori, R. Spagna, *J. Appl. Crystallogr.* **1999**, *32*, 115–119.
[50] SHELXL-97: G. M. Sheldrick, University of Göttingen, Germany, **1997**.
[51] T. J. B. Holland, S. A. T. Redfern, *Min. Mag.* **1997**, *61*, 65–77.
[52] CrystalDiffract 4.0.2 (CrystalMaker software).

Received: October 31, 2005
Published online: February 21, 2006

